Chapter 2

Nanofiber Filaments Fabricated by a Liquid-Bath Electrospinning Method

Long Tian, Tao Yan, Jie Li and Zhijuan Pan

Additional information is available at the end of the chapter

http://dx.doi.org/10.5772/intechopen.75197

Abstract

In order to investigate the forming process of multi-needle liquid-bath electrospun nanofiber filaments, nanofiber filaments were prepared using the multi-needle liquid-bath electrospinning method in this chapter. The effect of auxiliary electrode on jet state, and bundling and drawing processes of nanofibers were studied. The results show that the forming process of nanofiber filaments was mainly influenced by electrostatic field interference, bundling process, and drawing process, including two processes: forming process of as-spun nanofiber filaments and post-drawing process. In the forming process of as-spun nanofiber filaments, when the auxiliary electrode was added, the electrostatic field interference between needles reduced, inducing the decrease of jet offsets and the enhancement of Taylor cone and jet stability, and nanofibers with skin-core structure were finally deposited on the bath in good condition. The bundling process of nanofiber filament was divided into three processes: wet process, wet-dry process, and dry process; the structure transformation of nanofiber filaments mainly occurred in the wet process. In the post-drawing process, the crystallinity and alignment degree of nanofibers increased, and nanofiber diameter decreased. The initial modulus and breaking stress of filaments increased while the breaking strain of filaments decreased. Finally, nanofiber filaments were produced with better structures and properties.

Keywords: multi-needle, electrospinning, nanofiber filaments, forming process

1. Introduction

Nanofibers, characterized by a high surface-to-volume ratio and great flexibility [1, 2], have shown wide application in areas such as biomedical engineering, filtration, and electronic engineering [3, 4]. Electrospinning is an efficient technique to produce polymeric nanofibers [5, 6]. Most electrospun nanofibers are collected in the form of nonwoven webs [7]. However,

nanofiber webs are deficient in mechanical strength due to the random orientations of the nanofibers [8, 9], which limits their application in areas such as artificial organs and protective clothing [10, 11]. Nanofiber filaments or yarns are expected to be one of the best approaches to solve this problem and uncover new opportunities for the development of 3D nanofibrous structures [10, 12]. However, problems such as lack of production continuity and low mechanical strength still exist in current nanofiber filaments development.

In recent years, many methods have been developed to directly electrospin nanofibers into nanofiber filaments or yarns [12], such as using the self-assembly [13], the dual electrodes [14], the air assistant twisting device [15], the liquid bath collector [16, 17] and the rotary intermediate collecting device [11, 12, 18]. Among them, liquid-bath electrospinning method is regarded as one of the most efficient ways to produce nanofiber filaments, due to its better stability, continuity and applicability. Smit [16], Khil [19], and Pan et al. [20, 21] have successfully electrospun nanofiber filaments continuously by the liquid-bath electrospinning technique. However, there is no record about the forming process and mechanism of nanofiber filaments fabricated by liquid-bath electrospinning method.

Therefore, in this chapter, nanofiber filaments were prepared by liquid-bath electrospinning method with multi-needle. Then, the forming and post-drawing process of nanofiber filaments were studied, and the effects of electrostatic field interference, bundling process and drawing process on forming process of nanofiber filaments were emphatically discussed. Nanofiber filaments with better structures and properties could be achieved through this study. Meanwhile, this study could lay the theoretical and experimental foundation of the continuous manufacture of nanofiber filaments fabricated by liquid-bath electrospinning method with multi-needle.

2. Experimental

2.1. Materials

Pure PA6 pellets (product number 181110) were obtained from Sigma-Aldrich, and 88-wt% formic acid, purchased from Shanghai Chemical Reagent Co., Ltd., was chosen as the solvent. PA6 solutions were prepared by dissolving PA6 pellets into the solvent with continuous stirring at room temperature. The concentration of the PA6 solution was 25 wt%.

The bath solution was prepared by dissolving Peregal O (Jiangsu Jiafeng Chemical Co. Ltd.) into deionized water at room temperature, and the concentration of Peregal O solution was 0.5 wt% [21].

2.2. Filament manufacture

A homemade multi-needle liquid bath electrospinning device with an auxiliary electrode was used to continuously prepare the PA6 nanofiber filaments as in **Figure 1**. The PA6 solution was loaded into a syringe and then fed to the spinneret by the syringe pump. Both the spinneret

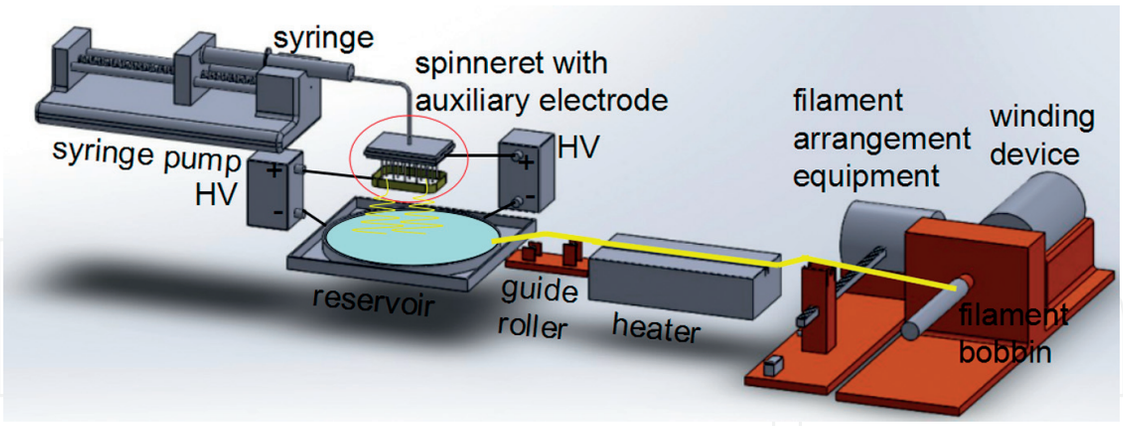

Figure 1. Schematic diagram of continuous and stable fabrication process of as-spun nanofiber filament by multi-needle electrospinning device with liquid-bath collector.

Voltage	**Flow rate**	**Vertical distance between the needle tip and the bath surface**	**Drying device**	
			Length	**Temperature**
26 kV	1.5 mL/h	60 mm	200 mm	350°C
Rotation mandrel		Auxiliary electrode		
Diameter	Rotation speed	Size (length×width)	Height	Voltage
78 mm	588 m/h	100 mm×80 mm	17.5 mm	22 kV

Table 1. Parameters of multi-needle electrospinning process with liquid-bath collector.

and the auxiliary electrode were connected to the cathodes of high-power supplies by copper wires, while the anodes were inserted into the bottom of the bath reservoir. The as-formed high electrostatic field turned PA6 solution into nanofibers on the surface of the bath, which were initially assembled into a nanofiber filament in the bath with the guidance of a glass rod, and the filament then went through the guide roller, the heater and the filament arrangement equipment successively, before being wound on the filament bobbin in the rotation device. The as-spun nanofiber filament was continuously manufactured by the drawing force caused by the rotation of the filament bobbin [22]. The parameters of the electrospinning are listed in **Table 1**.

2.3. Post-drawing

The post-drawing process of as-spun PA6 nanofiber filaments was shown in **Figure 2**. As-spun nanofiber filaments were unwound from the unwinding roller (outer diameter = 8.2 mm) with a certain speed (v_w), then nanofiber filaments passed through a bath (0.5% Peregal O solution) for being swelled, and next traversed the drying device to obtain enough energy for nanofiber movement. Finally, nanofiber filaments were evenly wound (the speed of v_u) on an winding roller (outer diameter = 8.2 mm).

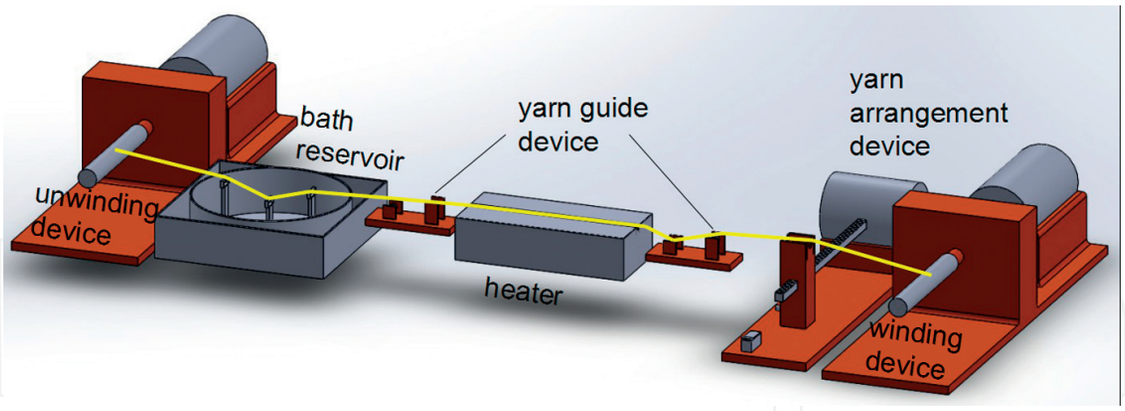

Figure 2. Schematic diagram of post-drawing device.

The post-drawing ratio (v_{draw}) could be determined by the speed ratio of winding roller and unwinding roller, as shown in Eq. 1.

$$v_{draw} = \frac{v_w}{v_u} \tag{1}$$

where v_w was the speed of winding roller, v_u was the speed of unwinding roller. Both parameters had the same unit of rotation per minute (rpm).

2.4. Characterization

The morphology of the nanofiber filaments was characterized by a scanning electron microscope (SEM) (Hitachi S-4800, Japan).

The diameters of the nanofibers in each yarn were determined by averaging 100 measurements of the nanofibers in the SEM images of the yarn using image analysis software (Image Pro Plus 5.0). Ten tensile-tested samples (length = 50 mm) were randomly selected from each tested filament. The diameter of each sample was obtained by averaging 10 measurements using a CU-2 fiber fineness tester. The diameter of each filament was obtained by averaging 10 samples' diameters.

The alignment degree (AD) of nanofiber filaments was characterized by the area ratio of aligned nanofibers and the yarn.

The mechanical properties of nanofiber filaments include initial modulus, breaking stress and strain. The measuring method was as following: first, 10 tensile-tested samples (length = 50 mm) were randomly selected from each tested filament and were maintained under standard conditions for 24 h before testing. The diameter of each sample (d_i) was obtained using a CU-2 fiber fineness tester. Second, the mechanical properties of each sample were then measured using an Instron 3365. The test parameters were set to a gauge length of 10 mm, crosshead speed of 10 mm/min, initial tension of 0.1 cN, and strength and elongation resolutions of 0.01 cN and 0.01 mm, respectively. Finally, the breaking strength (F_i), breaking length (l_i), and the strength with 1% extension (m_i) of each sample could be obtained. Therefore, the initial

modulus (M), breaking stress (δ), and strain (E) of each nanofiber filament were calculated according to Eqs. 2, 3, and 4 from the average of 10 samples:

$$M = \sum_{i=1}^{10} \frac{40m_i}{\pi d_i^2} \tag{2}$$

$$\delta = \sum_{i=1}^{10} \frac{2F_i}{5\pi d_i^2} \tag{3}$$

$$E = \sum_{i=1}^{10} \frac{l_i - 10}{100} \times 100\% \tag{4}$$

3. Results and discussion

3.1. Forming process of nanofiber filaments fabricated by liquid-bath electrospinning method with multi-needle

Forming process of nanofiber filaments fabricated by liquid-bath electrospinning method with multi-needle was as following: nanofibers were electrospun using polymer solution and collected on the bath, then experienced forming process based on wet spinning, and finally bundled into nanofiber filaments by tensile force. There exist electrostatic field interferences among multiple needles during electrospinning, which could disrupt the electrospinning process, leading to the uncontinuous manufacturing of nanofiber filaments. The best way to solve this problem was to add an auxiliary electrode to multi-needle. Therefore, the stable and continuous manufacture of nanofiber filaments by liquid-bath electrospinning method with multi-needle included four processes: (1) electrospinning, (2) weakening of electrostatic field interferences among multi-needle, (3) forming of nanofibers based on wet-spinning, and (4) bundling of nanofibers.

3.1.1. Electrospinning process

In recent years, many researchers have explored and built relatively complete theoretical system of electrospinning, based on physical theories of high-voltage electrostatic field and polymer solution. In high-voltage electrostatic field, there are three processes turning polymer solution into nanofibers: (1) forming of Taylor cone, (2) straight jet, and (3) bending instability, as shown in **Figure 3**.

3.1.2. Weakening process of electrostatic field interferences among multi-needle

Electrostatic field interferences could affect electrospinning and bundling process, by affecting the electrostatic field distribution and electrospinning jets. Therefore, an auxiliary electrode was needed to weaken electrostatic field interferences.

Higher electrostatic field interferences increased the instability of Taylor cones and jets, and jet whipping during the electrospinning process got more complex [23]. These two behaviors

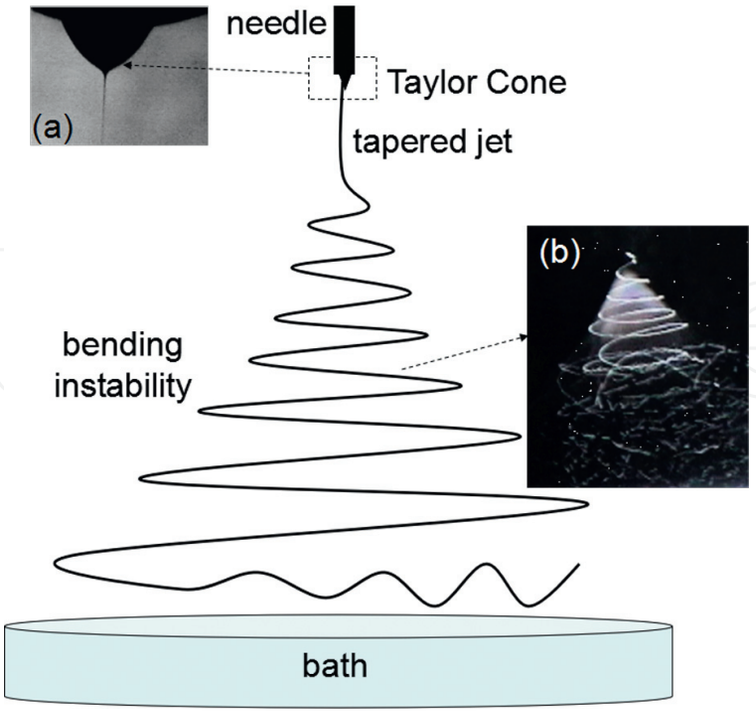

Figure 3. Schematic diagram of electrospinning process, (a) Taylor cone and straight segment, (b) bending instability.

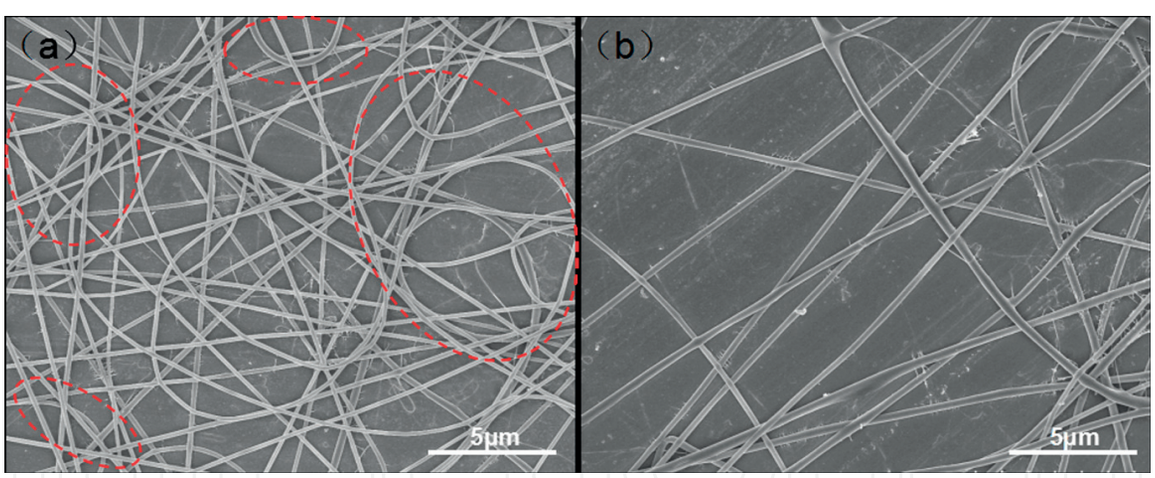

Figure 4. SEM images of nanofibers collected at the place which has a distance of 10 mm to needle tips during electrospinning process with and without rounded rectangular auxiliary electrode, (a) without auxiliary electrode, (b) with RAE.

would induce more irregular bends in the smooth nanofibers during flying, thereby leading to more intertwined and bent nanofibers, as shown in **Figure 4a**.

Higher electrostatic field interferences could also weaken electrostatic field intensity in the electrospinning space, thus resulting in the increase of nanofiber diameter due to weakened tensile force being applied to jets. Meanwhile, the offsets of jets (as shown in **Figure 5a**, 41.96° is the offset angle of the central needle in the left row) became larger, leading to larger distance

http://dx.doi.org/10.5772/intechopen.75197

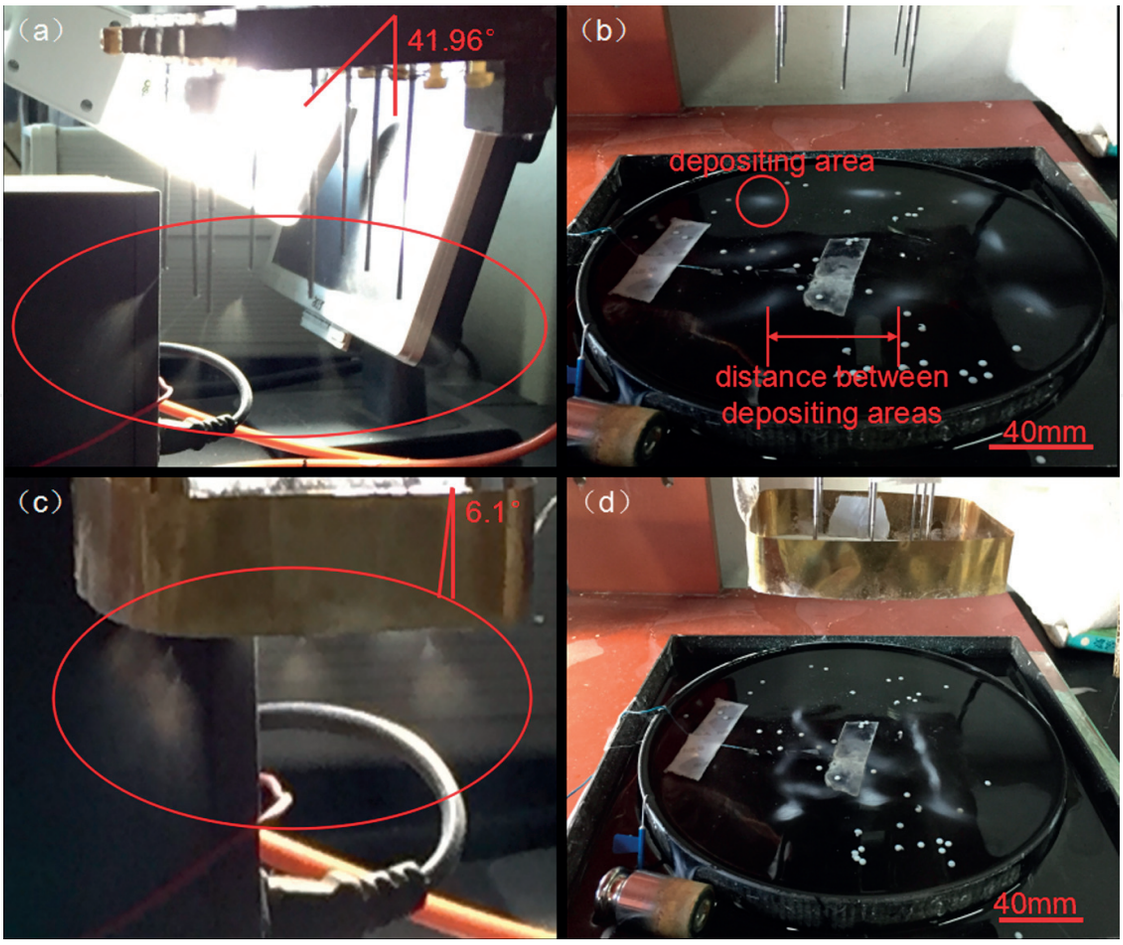

Figure 5. Effect of electrostatic field interference on electrospinning process, (a) jets state with higher electrostatic field interference, (b) nanofibers depositing state with higher electrostatic field interference, (c) jets state with lower electrostatic field interference, (d) nanofibers depositing state with lower electrostatic field interference.

between nanofiber depositing areas (the average distance between adjacent nanofiber depositing areas was 57.1 mm), which would affect bundling process of nanofiber filaments.

In this chapter, a round-corner rectangular auxiliary electrode (RAE) was applied during electrospinning process to weaken electrostatic field interferences. When electrostatic field interferences decreased, the instability of Taylor cones and jets was weakened. Meanwhile, the jet whipping during the electrospinning process also weakened [23]. Therefore, irregular bends in the smooth nanofibers during flying got less, thus resulting in less intertwined and bent nanofibers (as shown in **Figure 4b**).

With the decrease of electrostatic field interferences, the descending range of electrostatic field intensity decreased, resulting in smaller nanofiber diameter. Meanwhile, the offsets of jets decreased (as shown in **Figure 5b**, 6.1° is the offset angle of the central needle in the left row), inducing the decrease of distance between nanofiber depositing areas (the average distance between adjacent nanofiber depositing areas was 35.5 mm). Therefore, bundling process of nanofiber filament would be more stable and continuous.

3.1.3. Forming process of nanofibers based on wet spinning

Liquid-bath electrospinning nanofibers were collected in the bath, which is quite similar to coagulation bath during wet spinning. Therefore, whether this type of nanofibers had the typical structure of wet-spun fiber, skin core structure, was a subject worth exploring.

Nanofiber yarns (consisting of 12 nanofiber filaments) were overtwisted (3000 tpm, as shown in **Figure 6a**), thus the nanofibers became so stretched that they could be destroyed in this process, especially on their surfaces (as shown in **Figure 6b**). In order to explore the structures of the cracks, a slight tensile load was added to the nanofiber yarn, and the results were shown in **Figure 4c**. The structures of the surface and inner part of the nanofibers were different. This result indicated that the nanofibers had a skin core structure, which was also indicated by the cross section of the nanofibers in **Figure 4d**. This structure could be explained by the synthetic process of the nanofibers. The solvent evaporated from the nanofibers during the electrospinning before the flying nanofibers were collected in the bath, while there were still some solvent remaining in the fibers. Because the concentration of formic acid in the nanofibers was higher than that in the bath but the concentration of H_2O in the bath was higher than that in the nanofibers, counterdiffusion of these two solvents occurred in the surface of the deposited nanofibers when the nanofibers were deposited in the bath, thus forming a skin layer. Because the structure of the nanofiber skin was compact and dense, it hindered further counterdiffusion from occurring. The structure of the inner regions was therefore still loose and flexible, which lead to the skin core structure of the as-spun nanofibers [24–27].

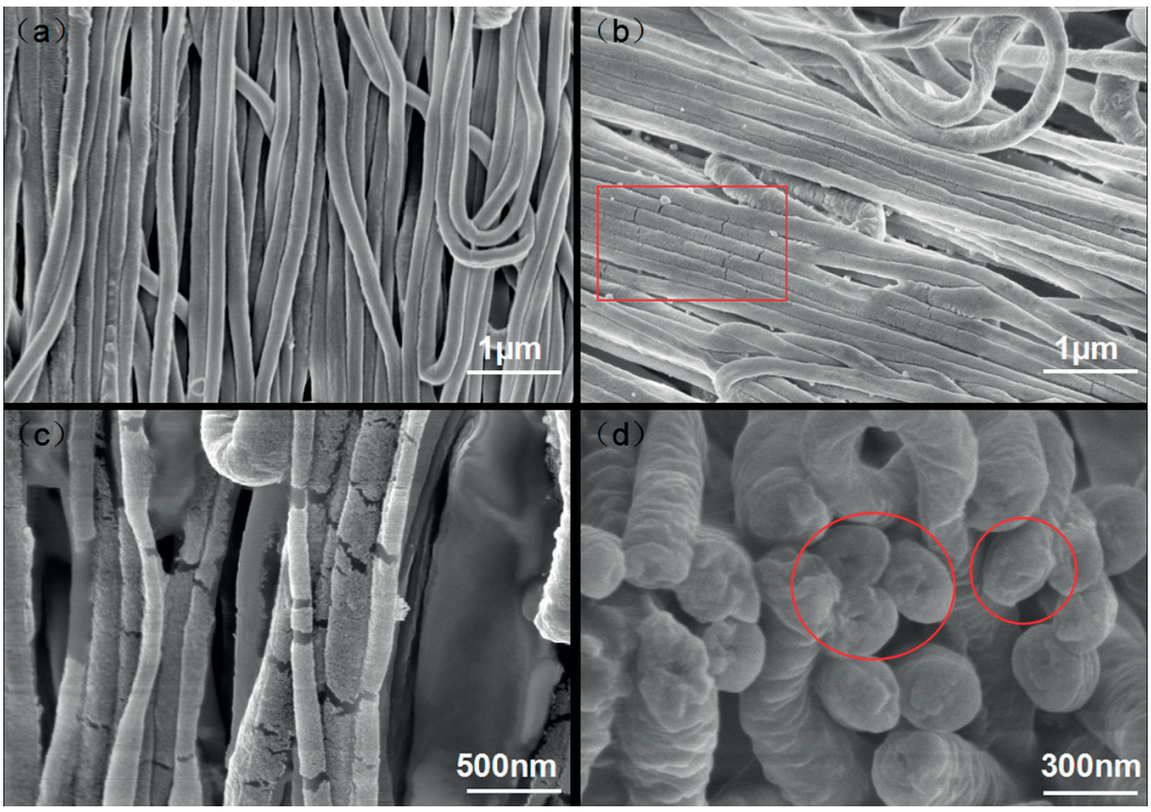

Figure 6. Skin core structure of nanofibers, (a) as-spun nanofiber filaments, (b) cracks on nanofiber surface after overtwisting, (c) nanofiber morphology after slight drawing, (d) cross sections of nanofibers.

3.1.4. Bundling process

The actual bundling process (as shown in **Figure 7a** and **b**) could be summarized as follows: electrospinning nanofibers were deposited on the bath in the form of lamelliform fiber assembly, then bundled under tensile force of winding roller and resistance force of bath, and next formed into a bundling triangular zone (as shown in **Figure 7c**) at the edge of bath reservoir turning the larger nanofiber bundle into a smaller wet one. The wet bundle then passed through the drying device becoming a dry bundle, and was finally wound on the winding roller forming the as-spun nanofiber filament. Therefore, the bundling process, as shown in **Figure 7d**, could be divided into three parts: wet process (as shown in **Figure 7a**), wet-dry process, and dry process (as shown in **Figure 7b**). Wet process consisted of transformation stage from lamelliform fiber assembly to bundling triangular zone and transformation stage from bundling triangular zone to wet bundle. Dry process consisted of transformation stage from dry bundle to as-spun filament.

3.1.4.1. Wet process

3.1.4.1.1. Transformation stage from lamelliform fiber assembly to bundling triangular zone

The nanofiber aggregative states of every process are shown in **Figure 8**. Nanofibers are randomly arranged in the lamelliform fiber assembly (as shown in **Figure 8a**), then moved into bundling triangular zone under the combined action of tensile force, water resistance force and interaction force between fibers. During this process, AD of the nanofiber bundle increased rapidly, but nanofiber diameter nearly kept the same, as shown in **Figure 9**. This is

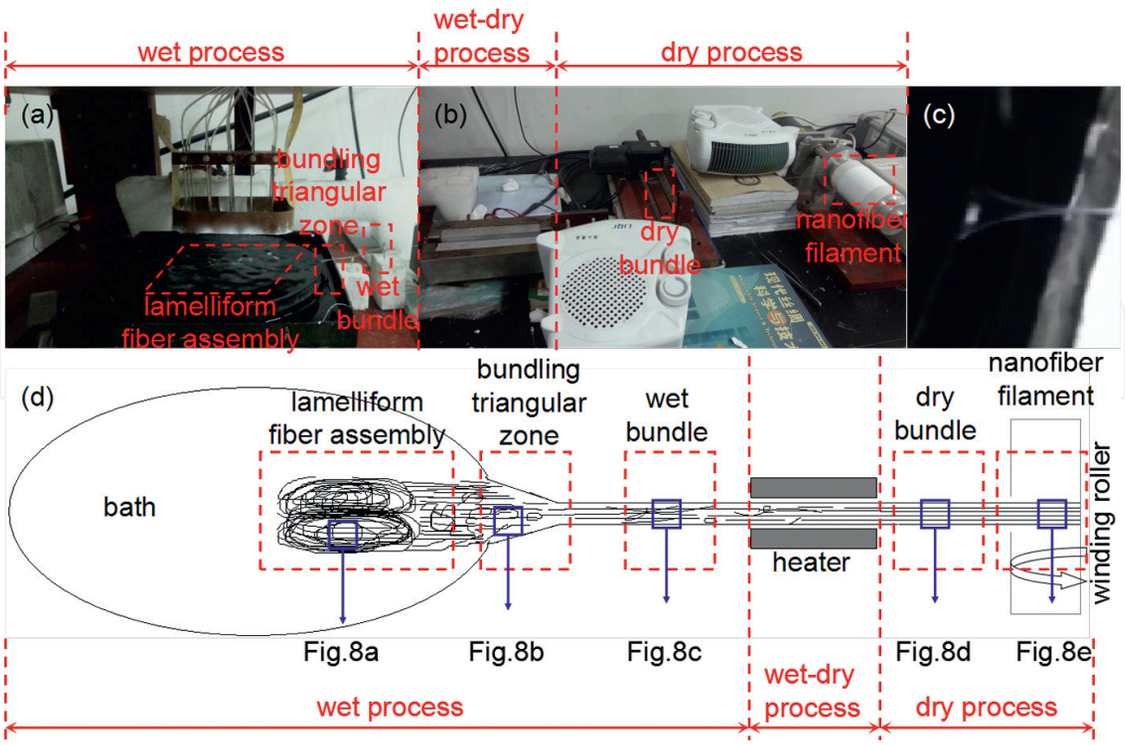

Figure 7. Bundling process of nanofiber filaments, (a) wet process, (b) wet-dry process, (c) bundling triangular zone, (d) schematic diagram of bundling process.

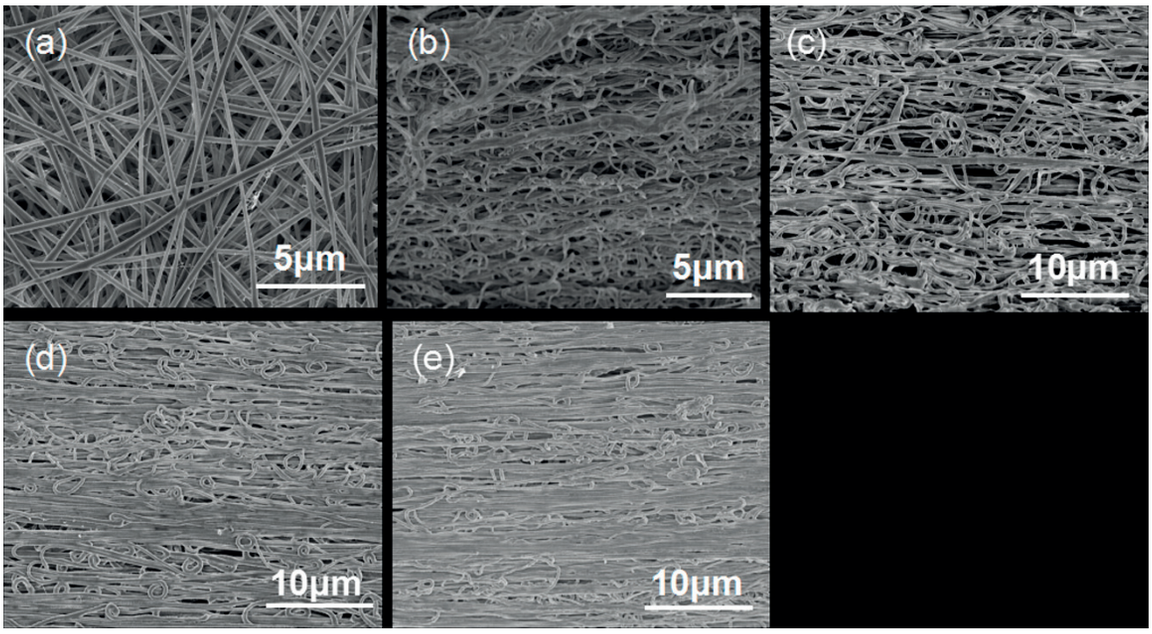

Figure 8. SEM images of nanofibers bundling morphologies during bundling process, (a) the lamelliform fiber assembly, (b) the bundling triangular zone, (c) the wet filament, (d) the dry filament, (e) the as-spun nanofiber filament.

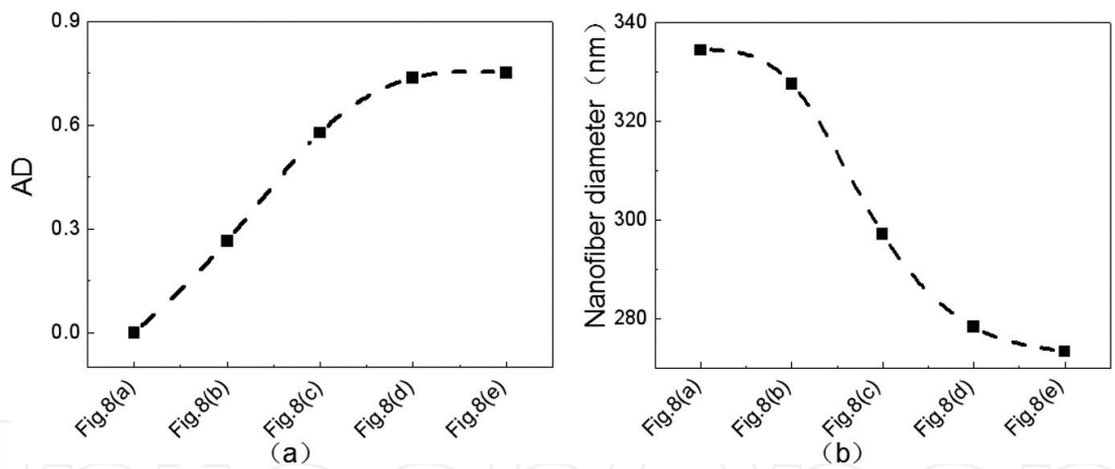

Figure 9. ADs and nanofiber diameters in nanofibers bundling states during bundling process, (a) ADs, (b) nanofiber diameters.

because the combined action was mainly contribute to the aligned movement of nanofibers, only minor combined force was used for nanofiber stretching. Although AD of nanofibers in bundling triangular zone was improved, the nonaligned nanofiber, like bent and hooked nanofibers, still occupied a dominant position, as shown in **Figure 8b**.

3.1.4.1.2. Transformation stage from bundling triangular zone to wet bundle process

Nanofibers moved forward from the bundling triangular zone to the wet bundle. During this process, a large number of nanofibers entered into a narrow space from a relatively large space, which increased the interaction force between nanofibers rapidly. Therefore, nanofibers

were immediately directionally arranged, and many bent and hooked nanofibers became straight (as shown in **Figure 8c**) under the combined force of tensile force, resistance force and interaction force between fibers; thus, AD of the wet bundle was enhanced sharply (as shown in **Figure 9a**). Meanwhile, nanofibers were stretched by the combined force, so the diameter of nanofibers decreased rapidly, as shown in **Figure 9b**.

3.1.4.2. Wet-dry process

Nanofibers continuously moved forward and passed through the dry device, forming a dry bundle. Before traversing the dry device, nanofibers in wet state could still be directionally arranged, straightened and stretched by the combined force. After drying, nanofibers' position and state were nearly fixed, thus the deformability of nanofibers was weakened. Therefore, both the increase of AD and the decrease of nanofiber diameter during this process were smaller than those during the previous process, as shown in **Figures 8d** and **9**.

3.1.4.3. Dry process

The dry bundle moved on and finally wound on the winding roller. As nanofibers were fixed in the bundle, the combined force could nearly make nanofibers be further aligned or stretched. Therefore, AD and diameter of nanofibers in the as-spun filament were nearly the same with those in the dry bundle, as shown in **Figures 8e** and **9**.

To sum up, the structure transformation of as-spun nanofiber filament, including the increase of AD and the decrease of nanofiber diameter, mostly took place during wet process.

Therefore, the forming mechanism of as-spun nanofiber filament could be summarized in **Figure 10**. Polymer solution was formed into drops on the tips of multiple needles by the syringe pump. In the high-voltage electrostatic field, the electrostatic field force applied to the drops could overcome their surface tension, so jets were ejected from the drops (Taylor cones). The jets flied towards the bath in the form of straight line initially, and then in the form of multistage open loop by the combined action of viscoelasticity, surface tension, coulomb force, electrostatic field force and multiple instability. By using the auxiliary electrode, the offsets of jets became smaller, the stability of Taylor cones and jets got better, and finally the jets turned into nanofibers depositing on the bath in better form. Then the lamelliform nanofiber assembly, formed based on wet spinning, began to be bundled by external force. It was bundled into wet bundle via bundling triangular zone at the edge of the bath reservoir, and then turned into dry bundle after drying, and finally formed into as-spun filament after winding.

3.2. Post-drawing process of as-spun nanofiber filaments

The structure and bundling state of nanofibers in filaments as well as the mechanical properties of nanofibers were unsatisfactory. The most efficient way to improve the structures and mechanical properties of filaments was to use post-drawing method. When an as-spun filament was drawn along its axis under a relatively high temperature (higher than the glass transition temperature of PA6), PA6 molecular chains could move and deform along its axis [28, 29], thus the internal structure, such as orientation and crystallinity degree, could be changed; meanwhile, nanofibers could also slip and deform along its axis, so the bundling

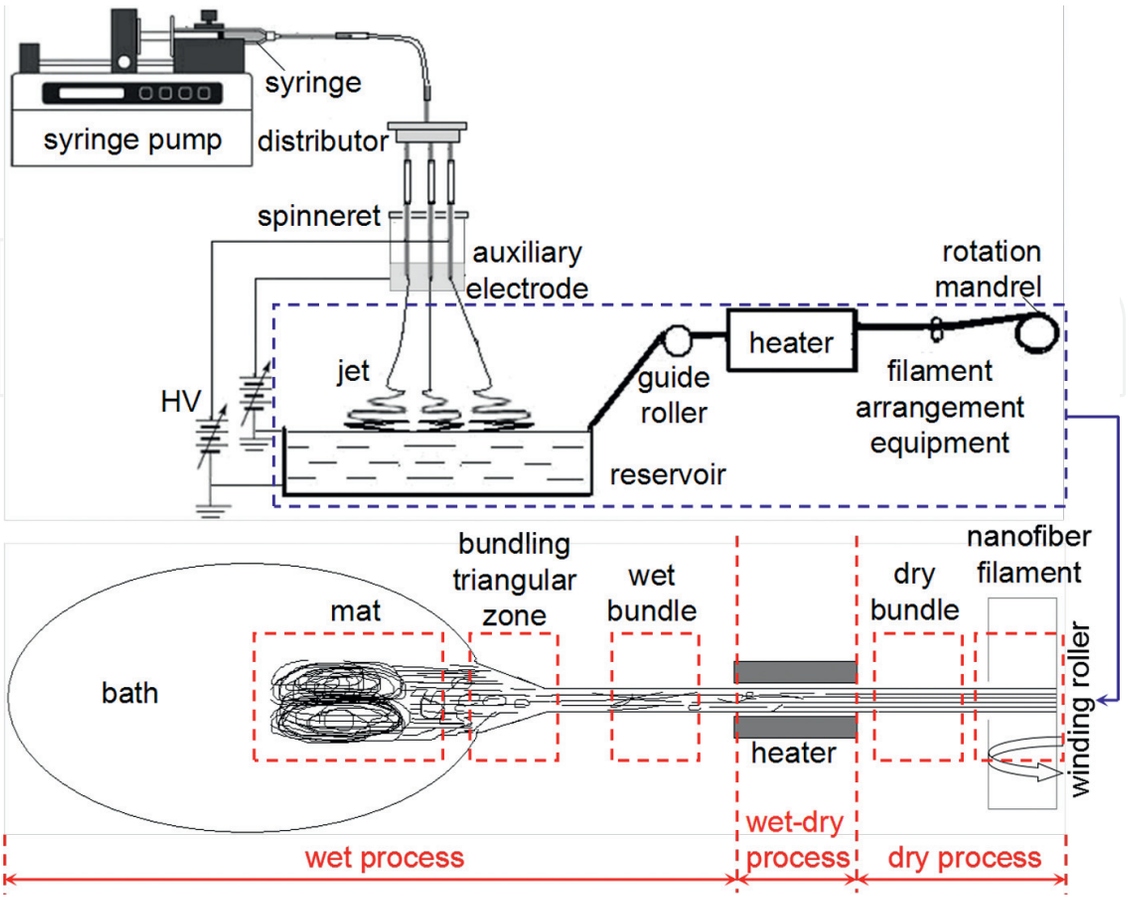

Figure 10. Schematic diagram of continuous and stable fabrication process by multi-needle electrospinning device using liquid-bath collector.

state of nanofibers in filaments could be improved. However, when the post-drawing ratio was very high, filaments were broken easily, which affected the continuous manufacture of filaments. Therefore, post-drawing ratios were selected as 1.2 times, 1.4 times and 1.6 times, to research the effect of post-drawing on structures and mechanical properties of filaments.

3.2.1. Effect of post-drawing on bundling states of filaments

Figure 11 shows bundling states of post-drawn filaments using different drawing ratios. With the increase of drawing ratios, the bent and hooked nanofibers reduced obviously, the structures of filaments got more compact, nanofiber diameter presented a decreasing trend, and ADs of filaments increased (as shown in **Figure 12**). Under a larger tensile force of post-drawing, more bent and hooked nanofibers could be straightened and obtain more plastic deformation [30], which makes nanofibers better aligned and thinner. Meanwhile, the larger tensile force could lead to more inter-fiber slippage, resulting in larger frictional force between the adjacent nanofibers, which helped more bent and hooked nanofibers to be straightened and stretched along the filament axis. Therefore, when post-drawing ratios increased, nanofiber diameters decreased, nanofiber bundling states were improved, and AD increased.

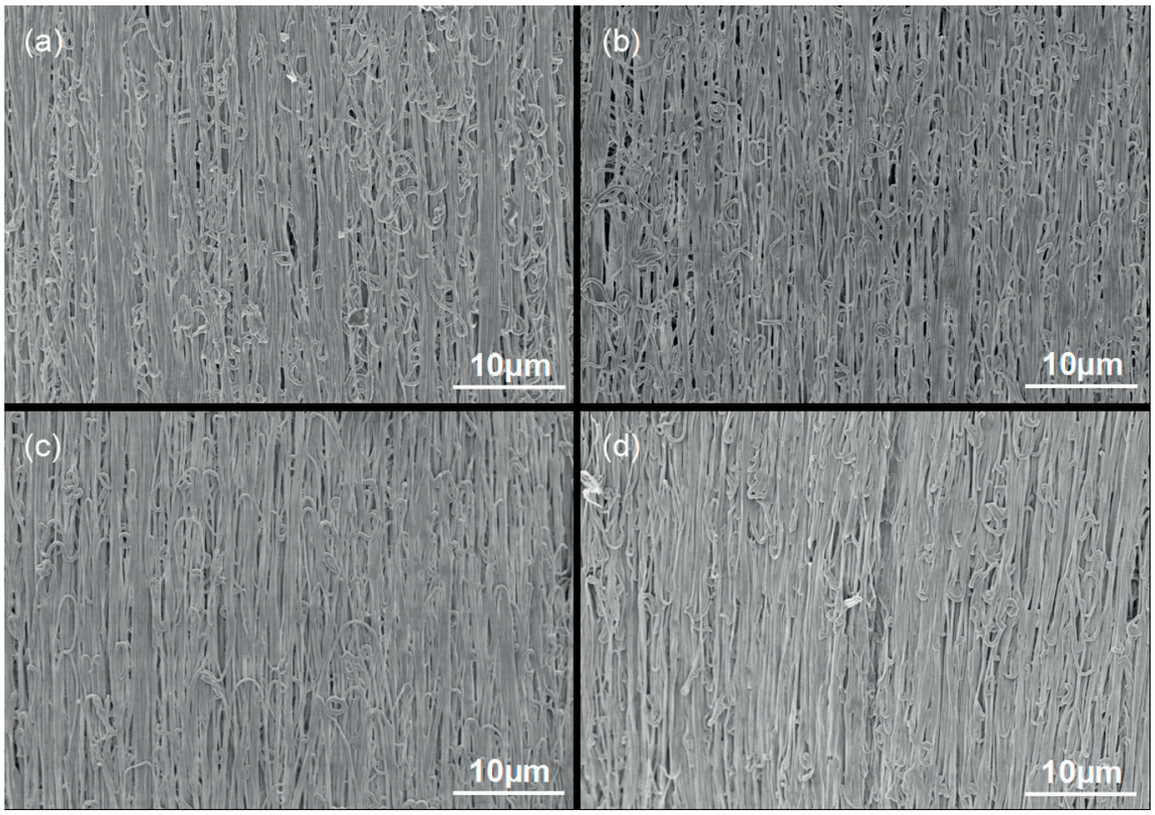

Figure 11. SEM images of nanofiber filaments post-drawn with different ratios, (a) without post-drawing (1.0 time), (b) 1.2 times, (c) 1.4 times, (d) 1.6 times.

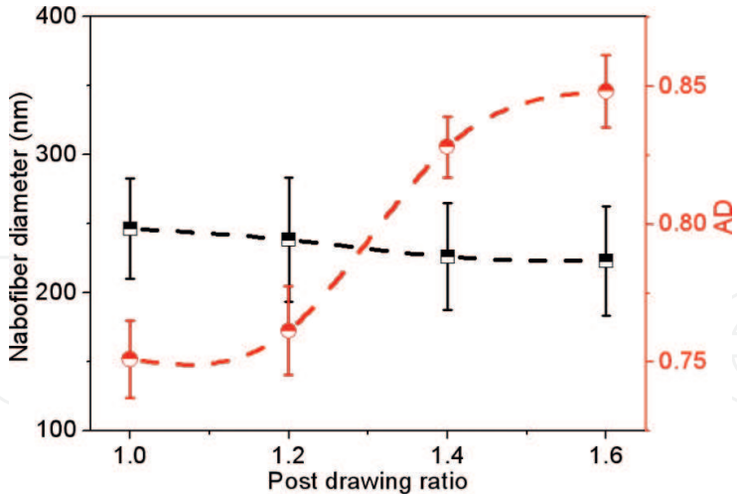

Figure 12. Nanofiber diameters and ADs of post-drawn filaments with different ratios.

3.2.2. Effect of post-drawing on crystalline structures of filaments

Figure 13 shows the crystalline structures of post-drawn filaments with different drawing ratios. It could be clearly observed that all post-drawn filaments exhibited the same diffraction peaks at the 2θ angles of 20.5°, 21.5° and 24.5° in **Figure 13a**. 20.5° and 24.5° represent α crystal and are

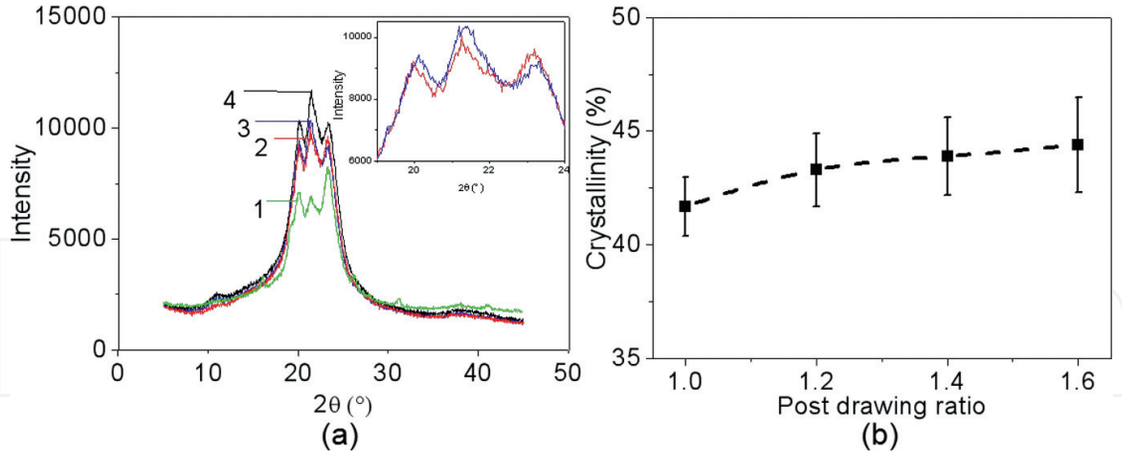

Figure 13. Crystallinities of nanofibers in filaments post-drawn with different ratios, (a) XRD curves, (b) crystallinities.

indexed as (200) and (002)/(202) reflections, respectively; while 21.5° represents γ crystal and are indexed as (001) reflections [31, 32]. This behavior indicated that post-drawing process did not change the crystalline structure of the filaments. However, the intensity of the diffraction peak of filaments became stronger with the increase of drawing ratios, especially at the 2θ angle of 21.6°, which indicated increase in crystallinities of filaments (as shown in **Figure 13b**). When post-drawing ratios increased, which meant larger tensile force was applied to filaments, more polymeric molecular chains in nanofibers could be more easily arranged regularly [33, 34], the distance between adjacent molecular chains decreased at the same time, so more hydrogen bonds between molecular chains could be formed in nanofibers, indicating the amount of γ crystal increased [35, 36]. In addition, some γ crystal could transform into α crystal under tensile force [37, 38]. Therefore, with the increase of drawing ratios, the crystallinities of filaments increased.

3.2.3. Effect of post-drawing on mechanical properties of filaments

Figure 14 shows stress–strain curves and main mechanical property indexes of post-drawn filament with different drawing ratios. With the increase of drawing ratios, the initial modulus and breaking stress of filaments were both improved, while the breaking strain of filaments reduced. Those variation trends were codetermined by mechanical properties of nanofibers, interaction between nanofibers and AD of filaments. With increasing drawing ratios, the nanofiber crystallinities increased, which was beneficial to promoting the initial modulus and breaking stress of filaments, the breaking strain was reduced accordingly. For filaments, the effect of filament bundling state was dominated by filament mechanical properties. With increasing the drawing ratios, more inter-fiber slippages happened, leading to the decrease of inter-fiber gaps, thus structures of filaments became more compact, inducing the enhancement of cohesive force between nanofibers; meanwhile, more oblique, bent and hooked nanofibers were straightened and directionally arranged. Those behaviors all contributed to the increase of initial modulus and breaking stress, and the decrease of the breaking strain.

http://dx.doi.org/10.5772/intechopen.75197

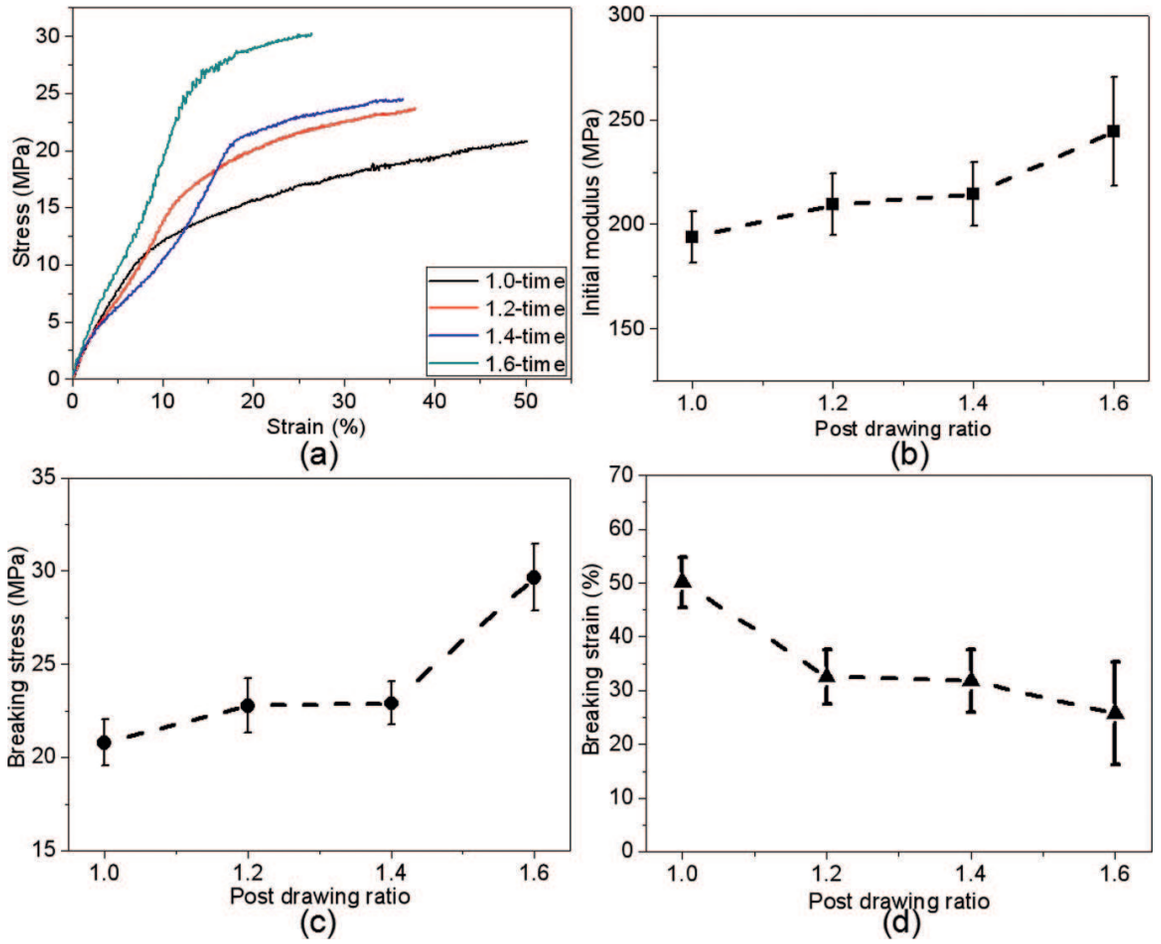

Figure 14. Mechanical properties of filaments post-drawn with different ratios, (a) stress–strain curves, (b) initial modulus, (c) breaking stress, (d) breaking strain.

4. Conclusion

The forming process of nanofiber filaments included two processes: forming process of as-spun nanofiber filaments and post-drawing process. In the forming process of as-spun nanofiber filaments, when the auxiliary electrode was added, the electrostatic field interference between needles reduced, inducing the decrease of jet offsets and the enhancement of Taylor cone and jet stability, and nanofibers with skin-core structure were finally deposited on the bath in good condition. The bundling process of nanofiber filament was divided into three processes: wet process, wet-dry process and dry process; the structure transformation of nanofiber filaments, including the increase of ADs and the decrease of nanofiber diameters, mainly occurred in the wet process. In the post-drawing process, the crystallinity and AD of nanofibers increased, and nanofiber diameter decreased. The initial modulus and breaking stress of filaments increased while the breaking strain of filaments decreased. Finally, nanofiber filaments were produced with better structures and properties.

Acknowledgements

Financial support for this work was provided by the Nantong Science and Technology Project (GY12016025).

Author details

Long Tian[1,2], Tao Yan[1], Jie Li[3] and Zhijuan Pan[1,2,4]*

*Address all correspondence to: zhjpan@suda.edu.cn

1 College of Textile and Clothing Engineering, Soochow University, Suzhou, China

2 Nantong Textile and Silk Industrial Technology Research Institute, Nantong, China

3 Jiangsu Textiles Quality Services Inspection Testing Institute, Nanjing, China

4 National Engineering Laboratory for Modern Silk, Soochow University, Suzhou, China

References

[1] Arinstein A, Zussman E. Electrospun polymer nanofibers: Mechanical and thermodynamic perspectives. Journal of Polymer Science Party B: Polymer Physics. 2011;**49**:691-707

[2] Del Gaudio C, Ercolani E, Nanni F, Bianco A. Assessment of poly (ε-caprolactone)/poly (3-hydroxybutyrate-co-3-hydroxyvalerate) blends processed by solvent casting and electrospinning. Materials Science and Engineering: A. 2011;**528**(3):1764-1772

[3] Su CI, Lai TC, Lu CH, Liu YS, Wu SP. Yarn formation of nanofibers prepared using electrospinning. Fibers and Polymers. 2013;**14**(4):542-549

[4] Fang J, Lin T, Tian W, Sharma A, Wang X. Toughened electrospun nanofibers from crosslinked elastomer-thermoplastic blends. Journal of Applied Polymer Science. 2007; **105**(4):2321-2326

[5] Konwarh R, Karak N, Misra M. Electrospun cellulose acetate nanofibers: The present status and gamut of biotechnological applications. Biotechnology Advances. 2013;**31**: 421-437

[6] Tungprapa S, Puangparn T, Weerasombut M, Jangchud I, Fakum P, Semongkhol S, et al. Electrospun cellulose acetate fibers: Effect of solvent system on morphology and fiber diameter. Cellulose. 2007;**14**(6):563-575

[7] Shuakat MN, Lin T. Recent developments in electrospinning of nanofiber yarns. Journal of Nanoscience and Nanotechnology. 2014;**14**:1389-1408

[8] Wu SH, Qin XH. Uniaxially aligned polyacrylonitrile nanofiber yarns prepared by a novel modified electrospinning method. Materials Letter. 2013;**106**:204-207

[9] Niu H, Gao W, Lin T, Wang X, Kong L. Composite yarns fabricated from continuous needleless electrospun nanofibers. Polymer Engineering & Science. 2014;**54**(7):1495-1502

[10] Hajiani F, Jeddi AAA, Gharehaghaji AA. An investigation on the effects of twist on geometry of the electrospinning triangle and polyamide 66 nanofiber yarn strength. Fibers and Polymer. 2012;**13**:244-252

[11] Li N, Hui Q, Xue H, Xiong J. Electrospun polyacrylonitrile nanofiber yarn prepared by funnel-shape collector. Materials Letter. 2012;**79**:245-247

[12] Ali U, Zhou Y, Wang X, Lin T. Direct electrospinning of highly twisted, continuous nanofiber yarns. Journal of Textile Institute. 2012;**103**:80-88

[13] El-Aufy AK. Nanofibers and Nanocomposites Poly(3,4-Ethylene Dioxythiophene)/Poly (Styrene Sulfonate) by Electrospinning [Thesis]. Philadelphia: Drexel University; 2004

[14] Pan H, Li LM. Continuous aligned polymer fibers produced by a modified electrospinning method. Polymer. 2006;**47**:4901-4904

[15] Ko F, Gogotsi Y, Ali A, Naguib N, Ye H, Yang GL, et al. Electrospinning of continuous carbon nanotube-filled nanofiber yarns. Advanced Materials. 2003;**15**(14):1161-1165

[16] Smit E, Buttner U, Sanderson RD. Continuous yarns from electrospun fibers. Polymer. 2005;**46**:2419-2423

[17] Teo WE, Gopal R, Ramaseshan R, Fujihara K, Ramakrishna S. A dynamic liquid support system for continuous electrospun yarn fabrication. Polymer. 2007;**48**(12):3400-3405

[18] Dabirian F, Ravandi SH, Sanatgar RH, Hinestroza JP. Manufacturing of twisted continuous PAN nanofiber yarn by electrospinning process. Fibers and Polymers. 2011;**12**(5):610-615

[19] Khil MS, Bhattarai SR, Kim HY, Kim SZ, Lee KH. Novel fabricated matrix via electrospinning for tissue engineering. Journal of Biomedical Materials Research Part B: Applied Biomaterials. 2005;**72**(1):117-124

[20] Liu Y, Li J, Pan ZJ. Effect of spinning conditions on the mechanical properties of PA6/MWNTs nanofiber. Journal of Polymer Research. 2011;**18**(6):2055-2060

[21] Li J, Tian L, Pan N, Pan ZJ. Mechanical and electrical properties of the PA6/SWNTs nanofiber yarn by electrospinning. Polymer Engineering & Science. 2014;**54**(7):1618-1624

[22] Tian L, Zhao C, Pan Z. Fabrication of high-alignment-degree nanofiber filaments using multi-needle electrospinning equipment with an auxiliary electrode. Science of Advanced Materials. 2015;**7**(11):2327-2335

[23] Karatay O, Dogan M, Uyar T, Cokeliler D, Kocum IC. An alternative electrospinning approach with varying electric field for 2-D-aligned nanofibers. IEEE Transactions on Nanotechnology. 2014;**13**(1):101-108

[24] Ge H, Liu H, Chen J, Wang C. The skin-core structure of poly (acrylonitrile-itaconic acid) precursor fibers in wet-spinning. Journal of Applied Polymer Science. 2008;**108**(2):947-952

[25] Lv M, Ge H, Chen J. Study on the chemical structure and skin-core structure of polyacrylonitrile-based fibers during stabilization. Journal of Polymer Research. 2009;**16**: 513-517

[26] Kitagawa T, Yabuki K, Young RJ. An investigation into the relationship between processing, structure, and properties for high-modulus PBO fibers. II. Hysteresis of stress-induced Raman band shifts and peak broadening, and skin-core structure. Journal of Macromolecular Science, Part B. 2002;**41**(1):61-76

[27] Wang M, Jin HJ, Kaplan DL, Rutledge GC. Mechanical properties of electrospun silk fibers. Macromolecules. 2004;**37**:6856-6864

[28] Barkoula NM, Peijs T, Schimanski T, Loos J. Processing of single polymer composites using the concept of constrained fibers. Polymer Composites. 2005;**26**(1):114-120

[29] Rongved L, Kurjian C, Geyling F. Mechanical tempering of optical fibers. Journal of Non-Crystalline Solids. 1980;**42**(1):579-584

[30] Butler R, Prevorsek D, Kwon Y. Optimization of fiber drawing processes in terms of the filament state variables. Polymer Engineering & Science. 1982;**22**(6):329-344

[31] Zhao Z, Zheng W, Tian H, Yu W, Han D, Li B. Crystallization behaviors of secondarily quenched nylon 6. Materials Letters. 2007;**61**(3):925-928

[32] Tian L, Zhao C, Li J, Pan Z. Multi-needle, electrospun, nanofiber filaments: Effects of the needle arrangement on the nanofiber alignment degree and electrostatic field distribution. Textile Research Journal. 2015;**85**(6):621-631

[33] Pan ZJ, Liu HB, Wan QH. Morphology and mechanical property of electrospun PA 6/66 copolymer filament constructed of nanofibers. Journal of Fiber Bioengineering and Informatics. 2008;**1**(1):47-54

[34] Xie Z, Niu H, Lin T. Continuous polyacrylonitrile nanofiber yarns: Preparation and dry-drawing treatment for carbon nanofiber production. RSC Advances. 2015;**5**(20):15147-15153

[35] Kim GM, Michler GH, Ania F, Calleja FB. Temperature dependence of polymorphism in electrospun nanofibres of PA6 and PA6/clay nanocomposite. Polymer. 2007;**48**(16):4814-4823

[36] Stephens JS, Chase DB, Rabolt JF. Effect of the electrospinning process on polymer crystallization chain conformation in nylon-6 and nylon-12. Macromolecules. 2004;**37**(3):877-881

[37] Ibanes C, De Boissieu M, David L, Seguela R. High temperature behaviour of the crystalline phases in unfilled and clay-filled nylon 6 fibers. Polymer. 2006;**47**(14):5071-5079

[38] Miri V, Persyn O, Lefebvre JM, Seguela R, Stroeks A. Strain-induced disorder–order crystalline phase transition in nylon 6 and its miscible blends. Polymer. 2007;**48**(17):5080-5087